Molecular Crystals and Liquid Crystals

ISSN: 1542-1406 (Print) 1563-5287 (Online) Journal homepage: http://www.tandfonline.com/loi/gmcl20

The effect of position of tert-butyl tail group on the formation of liquid crystal in Schiff base ester based homologous series

V. S. Sharma & R. B. Patel

To cite this article: V. S. Sharma & R. B. Patel (2017) The effect of position of tert-butyl tail group on the formation of liquid crystal in Schiff base ester based homologous series, Molecular Crystals and Liquid Crystals, 648:1, 53-65, DOI: 10.1080/15421406.2017.1283886

To link to this article: http://dx.doi.org/10.1080/15421406.2017.1283886

Published online: 28 Jun 2017.

MOLECULAR CRYSTALS AND LIQUID CRYSTALS
2017, VOL. 648, 53–65
https://doi.org/10.1080/15421406.2017.1283886

Taylor & Francis
Taylor & Francis Group

The effect of position of *tert*-butyl tail group on the formation of liquid crystal in Schiff base ester based homologous series

V. S. Sharma and R. B. Patel

Chemistry Department, K. K. Shah Jarodwala Maninagar Science College, Gujarat University, Ahmedabad, Gujarat, India

ABSTRACT

We report a newly rod like calamatic liquid crystalline materials, which are constructed by the self-organization of a rod-like carboxylic acid derivative based on Schiff base ester as the linking group with tert butyl tail group. A newly series of 4-(*tert*-butyl) phenyl 4-((4-alkoxybenzylidene) amino) benzoate with different alkyl chain spacer (n = 1 to 8, 10, 12, 14, 16, and 18) were synthesized and their mesomorphic properties were investigated by differential scanning calorimetry and polarized optical microscopy. All homologous in present series displays mesophase in enantiotropically manner. Thermal stability of SmC-SmA is 137.5 °C. All the compounds were characterized by spectroscopic and elemental analysis. The effects of varying left alkyl side spacer on mesomorphism with its structurally related compounds in series have been discussed.

KEYWORDS

Liquid crystal; smectic; enantiotropic; Schiff base

GRAPHICAL ABSTRACT

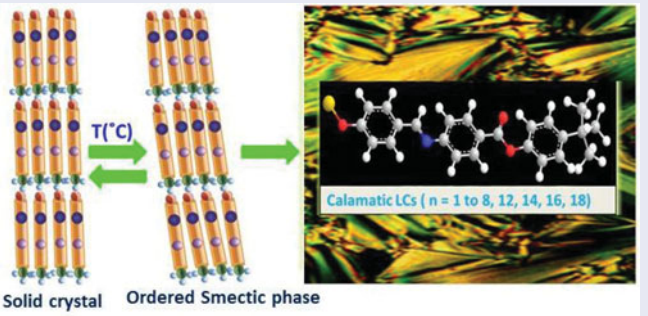

1. Introduction

The mesomorphic behavior of an organic compound is sensitive to its molecular architecture; a slight change in the molecular geometry brings about considerable change in its mesomorphic properties. The detailed study of many mesogenic homologous series has helped to evolve some general rules for the effect of chemical constitution in the nematogenic and smectogenic compounds [1–2]. Schiff base compounds are widely used in many fields, such as

CONTACT Vinay. S. Sharma vinaysharma3836@gmail.com Chemistry Department, K. K. Shah Jarodwala Maninagar Science College, Gujarat University, Ahmedabad 380008, Gujarat, India.
Color versions of one or more of the figures in the article can be found online at www.tandfonline.com/gmcl.

catalytic chemistry [3], organometallic chemistry [4], biochemistry [5], and photochemistry [6]. Schiff bases have attracted much attention in the field liquid crystal researches since the first report on the Schiff base liquid crystal compound 4-methoxybenzylidene-4'-butylaniline (MBBA) by Kelker et al. [7]. Over the past few decades, lots of Schiff bases with low molecular weight have been synthesized and investigated extensively toward applications of liquid crystal [8–10]. Dave et al. have synthesized a number of 4-n-alkoxy-1-naphthylidene Schiff bases and cholesteryl naphthoates and studied their mesomorphism [11–12]. Sie et al. reported Schiff base and ester linking group based heterocyclic benzoxazole liquid crystal, they studied the compounds displayed enantiotropic smectic A phase [13]. Yeap et al. have synthesized and studied of 1,3, 5-trisubstituted benzene based star shaped derivatives containing Schiff base and ester linking group [14]. Ha et al. and his coworkers have synthesized a series of Schiff base ethers comprising a dimethyl amino group at one terminal position and an even number of carbons at the other along the molecular axis [15]. Lin et al. synthesized a new mesogenic schiff base esters contain polar chloro group at the end and two phenyl rings. [16]. Yeap reported Schiff base ester based N-[4-(4-n-Hexadecanoyloxy benzoyloxy)-Benzylidene]-4-subtituted anilines [17]. Huang et al. reported Schiff base liquid crystal contains (S)-2-octyloxy tail and studied the effect of tail on the formation of frustrated blue phase and antiferroelectric phase [18]. The mesomorphic properties of aromatic Schiff base esters arising from substituents varying in their polarities have been reported by Ha et al. [19]. Many mesogenic homologous series contain two central linkages, one of which may be ester and the other azomethine [20–21]. Yellamaggad et al. reported in 2007 to synthesized six homologous series based on salicylaldimine based banana shaped mesogens derived from laterally substituted resorcinol [22].

Recently, Bhoya et al. synthesized Schiff base cinnamate based homologous series and studied the effect of ortho substituted bromo group on mesomorphism [23]. Doshi et al. reported homologous series contain ester and vinyl ester linkage group [24–25]. Previously, our research group reported various homologous series based on 4-n-alkoxy benzoates and Trans 4-n-alkoxy cinnamate derivatives linking with other chalconyl derivatives and studied the effect of tail or lateral group on mesomorphism [26–30].

2. Experimental

2.1. Materials

For present synthesized homologous series required materials: 4-hydroxy benzaldehyde, 4-amino benzoic acid purchased from (S.R.L, Mumbai), para *tert*-Butyl phenol were purchased from (Sigma Aldrich). Anhydrous K_2CO_3 was purchased from (Finar Chemical, Ahmedabad), N, N-dimethyl amino pyridine (DMAP) and Dicyclohexylcarbodiimide (DCC) was purchased from (Fluka Chemie, Switzerland). Alkyl bromides (R-Br) were purchased from S.R.L. Chemicals (Mumbai). All solvents were dried and purified by standard method prior to use.

2.2. Measurements

Melting points were taken on Opti-Melt (Automated melting point system). The FT-IR spectra were recorded as KBr pellet on Shimadzu in the range of 3800–600 cm^{-1}. Microanalysis was performed on Perkin-Elmer PE 2400 CHN analyzer. The texture images were studied on

a trinocular optical polarizing microscope (POM) equipped with a heating plate and digital camera. ^{1}H NMR spectra was recorded on a 400 MHz in Bruker Advance 400 in the range of 0.5–16 ppm using $CDCl_3$ as solvent. The phase transition temperatures were measured using Shimadzu DSC-50 at heating and cooling rates of 10 °C min^{-1}. Texture image of nematic phase were determined by miscibility method. Thermodynamic quantities enthalpy (ΔH) and entropy ($\Delta S = \Delta H/T$) are qualitatively discussed. For the POM study, novel synthesized compound is sandwiched between glass slide and cover slip and heating and cooling rate is (2 °C/min), respectively.

2.3. Synthesis

4-n-Alkoxy benzaldehyde (A) was prepared by reported method [31]. 4-((4-Alkoxy benzylidene) amino) benzoic acid (B) was prepared by usual established method [32]. Esters (C_1 to C_8, C_{10}, C_{12}, C_{14}, C_{16}, and C_{18}) were synthesized by a reported method in literature [33]. Thus, the synthesized target compounds were filtered, washed, dried and purified till constant transition temperatures is obtain, using an optical polarizing microscope equipped with a heating stage. The synthetic route to a series is mentioned in Scheme 1.

2.3.1. Synthesis of 4-n-alkoxy benzaldehyde (A)

4-n-Alkoxy benzaldehyde (A) was synthesized by refluxing the mixture of 4-hydroxy benzaldehyde (1 equiv.) with corresponding n-alkyl bromide (R-Br) (1 equiv.) in presence of anhydrous K_2CO_3 (1 equiv.) in dry acetone as a solvent [31].

2.3.2. 4-((4-Alkoxy benzylidene) amino) benzoic acid (B)

4-((4-Alkoxy benzylidene) amino) benzoic acid was prepared by refluxing the mixture of (A) and 4-amino benzoic acid at 3 to 4 hours in presence of ethanol and few drops of acetic acid [32]. The resultant mixture was filtered, dried, and purified by column chromatography which was confirmed by IR and ^{1}H NMR analysis.

2.3.3. Synthesis of 4-(tert-butyl) phenyl 4-((4-n-alkoxy benzylidene) amino) benzoate (C)

4-(Tert-butyl) phenyl 4-((4-n-alkoxy benzylidene) amino) benzoate (C) was prepared by esterification of (B) and 4-*tert* butyl phenol by usual established method reported in literature [33]. The appropriate (B) (2.02 mmol) and 4-*tert* butyl phenol (C) (0.246 g, 2.02 mmol), dicyclohexylcarbodiimide (DCC) (0.457 g, 2.22 mmol) and dimethylaminopyridine (DMAP) in catalytic amount (0.002 g, 0.2 mmol) in dry CH_2Cl_2 (DCM) (30 ml) was stirred at room temperature for 48 hr. The white precipitate of DCU is obtained which was isolated by filtration and discarded, while the filtrate was evaporated to dry. The resultant crude product was purified by column chromatography on silica gel eluting with dichloromethane: methanol and recrystallization from methanol: chloroform (2:4) until the constant transition temperatures were observed.

2.3.4. Reaction scheme

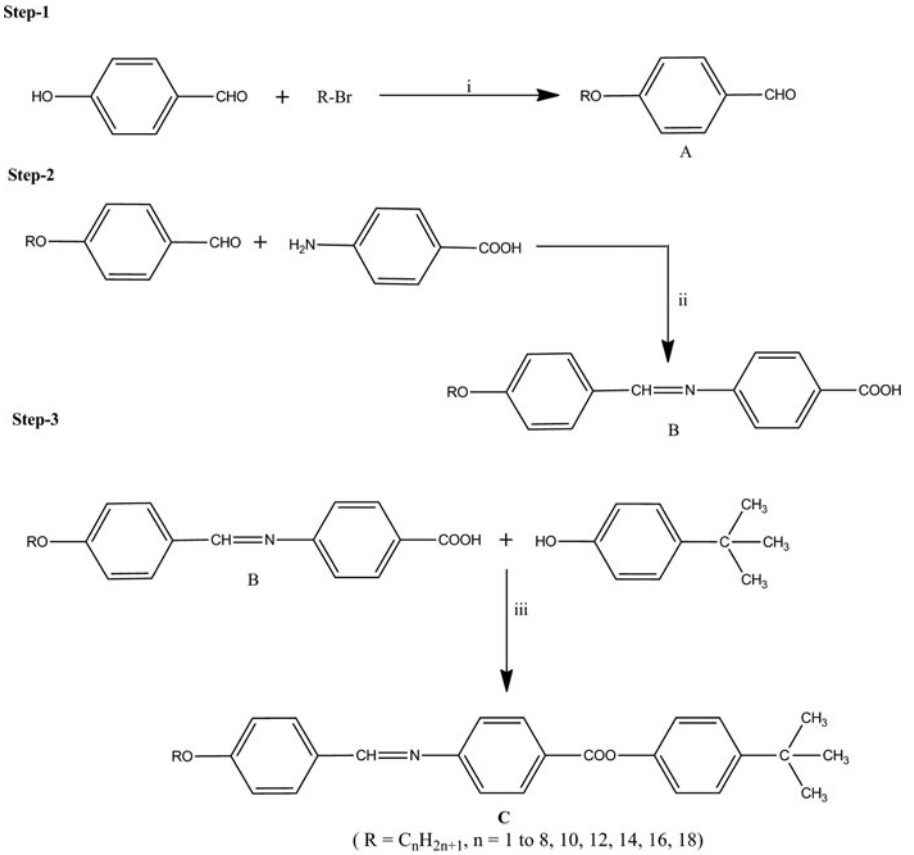

Scheme 1. Synthetic route of target compounds.

2.3.5. Analytical data

Compound (B_1): FT-IR (KBr) in cm^{-1}: 3032 (–C–H– Str in aromatic), 2825(C–H Str. in $–OCH_3$), 1365 and 1236 (–C–O Str), 806 disubstituted aromatic ring (–para), 1630 (–CH═N, Str. azomethine group), 1667 (–C═O Str.), 2550 (–OH of –COOH group). ^{1}H NMR: δH ($CDCl_3$, 400 MHz): 3.80 (s, 3H, $–CH_3$ of $–OCH_3$ group), 10.32 (s, 1H, –OH group of –COOH), 8.23 (s, 1H, –CH═N– group), 7.01–7.82 (4H, first phenyl ring), 7.42–8.14 (4H, second phenyl ring); Elemental analysis of $C_{15}H_{13}NO_3$: Calculate: C; 70.58%, H; 5.09%, O; 18.82%, N; 5.49%, Found: C; 69.62%, H; 4.96%, O; 18.74%, N; 5.42%.

Compound (B_{10}): FT-IR (KBr) in cm^{-1}: 3031 (–C–H– Str in aromatic), 681 Polymethylene $(–CH_2-)n$ of $–OC_{10}H_{21}$, 1355 and 1230 (–C–O str), 821 disubstituted aromatic ring (–para), 1630 (–CH═N, Str. azomethine group), 1661 (–C═O Str.), 2556 (–OH of –COOH group). ^{1}H NMR: δH ($CDCl_3$, 400 MHz): 0.88 (t, 2H, $–OC_{10}H_{21}$ group), 1.31 (q, 3H, $–OC_{10}H_{21}$ group), 1.26–1.29 (m, 12H, $–OC_{10}H_{21}$ group), 1.71 (P, 2H, $–OC_{10}H_{21}$ group), 4.06 (t, 2H, $–OC_{10}H_{21}$ group), 10.48 (s, 1H, –OH group of –COOH), 8.23 (s, 1H, –CH═N– group), 7.06–7.82 (4H,

first phenyl ring), 7.43–8.14 (4H, second phenyl ring); Elemental analysis of $C_{24}H_{31}NO_3$: Calcu: C; 75.59%, H; 8.13%, O; 12.59%, N; 3.67%, Found: C; 75.32%, H; 8.02%, O; 12.52%, N; 3.62%.

Compound (B_{12}): FT-IR (KBr) in cm^{-1}: 3032 (–C–H– Str in aromatic), 1365 and 1236 (–C–O str), 644 Polymethylene (–CH_2-)n of –$OC_{12}H_{25}$, 808 disubstituted aromatic ring (–para), 1631 (–CH═N, Str. azomethine group), 1672 (–C═O Str.), 2558 (–OH of –COOH group); ^{1}H NMR: 0.88 (t, 2H, –$OC_{12}H_{25}$ group), 1.31 (q, 3H, –$OC_{12}H_{25}$ group), 1.26–1.29 (m, 14H, –$OC_{12}H_{25}$ group), 1.71 (P, 2H, –$OC_{12}H_{25}$ group), 4.06 (t, 2H, –$OC_{12}H_{25}$ group), 10.68 (s, 1H, –OH group of –COOH), 8.21 (s, 1H, –CH═N– group), 7.04–7.81 (4H, first phenyl ring), 7.43–8.14 (4H, second phenyl ring); Elemental analysis of $C_{26}H_{35}NO_3$: Calcu: C; 76.28%, H; 8.55%, O; 11.73%, N; 3.42%, Found: C; 76.23%, H; 8.48%, O; 11.68%, N; 3.37%.

Compound (C_6): FT-IR (KBr) in cm^{-1}: 3032 (–C–H– Str in aromatic), 1365 and 1236 (–C–O str), 644 Polymethylene (–CH_2-)n of –OC_6H_{13}, 808 disubstituted aromatic ring (–para), 1620 (–CH═N, Str. azomethine group), 1661 (–C═O Str.), 2550 (–OH of –COOH group); ^{1}H NMR: δH ($CDCl_3$, 400 MHz): 0.88 (t, 3H, –CH_3 of –OC_6H_{13} group), 1.26–1.29 (m, 8H, –OC_6H_{13} group), 1.32 (s, 9H, –$C(CH_3)_3$ group), 1.73 (P, 2H, –CH_2- of –OC_6H_{13} group), 4.06 (t, 2H, –OCH_2- of –OC_6H_{13}), 8.31 (s, 1H, –CH═N group), 7.06–7.83 (4H, first phenyl ring), 7.32–8.16 (4H, second phenyl ring), 7.21–7.64 (4H, third phenyl ring); Elemental analysis of $C_{30}H_{35}NO_3$: Calcu: C; 78.77%, H; 7.65%, O; 10.50%, N; 3.06%, Found: C; 78.32%, H; 9.92%, O; 10.42%, N; 3.01%.

Compound (C_8): FT-IR (KBr) in cm^{-1}: 3030 (–C–H– Str in aromatic), 1342 and 1236 (–C–O str), 632 Polymethylene (–CH_2-)n of –OC_8H_{17}, 801 disubstituted aromatic ring (–para), 1631 (–CH═N, Str. azomethine group), 1672 (–C═O Str.), 2558 (–OH of –COOH group); ^{1}H NMR: δH ($CDCl_3$, 400 MHz): 0.88 (t, 3H, –CH_3 of –OC_8H_{17} group), 1.26–1.29 (m, 10H, –OC_8H_{17} group), 1.31 (s, 9H, –$C(CH_3)_3$ group), 1.73 (P, 2H, –CH_2- of –OC_8H_{17} group), 4.06 (t, 2H, –OCH_2- of –OC_8H_{17}), 8.34 (s, 1H, –CH═N group), 7.06–7.83 (4H, first phenyl ring), 7.32–8.16 (4H, second phenyl ring), 7.21–7.64 (4H, third phenyl ring); Elemental analysis of $C_{32}H_{39}NO_3$: Calcu: C; 79.17%, H; 8.04%, O; 9.89%, N; 2.88%, Found: C; 78.06%, H; 7.97%, O; 9.76%, N; 2.74%.

Compound (C_{10}): FT-IR (KBr) in cm^{-1}: 3031 (–C–H– Str in aromatic), 1365 and 1236 (–C–O str), 644 Polymethylene (–CH_2-)n of –$OC_{10}H_{21}$, 808 disubstituted aromatic ring (–para), 1631 (–CH═N, Str. azomethine group), 1672 (–C═O Str.), 2558 (–OH of –COOH group); ^{1}H NMR: δH ($CDCl_3$, 400 MHz): 0.88 (t, 3H, –CH_3 of –$OC_{10}H_{21}$ group), 1.26–1.29 (m, 12H, –$OC_{10}H_{21}$ group), 1.32 (s, 9H, –$C(CH_3)_3$ group), 1.73 (P, 2H, –CH_2- of –$OC_{10}H_{21}$ group), 4.06 (t, 2H, –OCH_2- of –$OC_{10}H_{21}$), 8.34 (s, 1H, –CH═N group), 7.06–7.83 (4H, first phenyl ring), 7.32–8.16 (4H, second phenyl ring), 7.20–7.62 (4H, third phenyl ring); Elemental analysis of $C_{34}H_{43}NO_3$: Calcu: C; 79.53%, H; 8.38%, O; 9.35%, N; 2.72%, Found: C; 79.42%, H; 8.29%, O; 9.27%, N; 2.68%.

Compound (C_{12}): FT-IR (KBr) in cm^{-1}: 3032 (–C–H– Str in aromatic), 1365 and 1236 (–C–O str), 644 Polymethylene (–CH_2-)n of –$OC_{12}H_{25}$, 808 disubstituted aromatic ring (–para), 1631 (–CH═N, Str. azomethine group), 1672 (–C═O Str.), 2552 (–OH of –COOH group); ^{1}H NMR: δH ($CDCl_3$, 400 MHz): 0.88 (t, 3H, –CH_3 of –$OC_{12}H_{25}$ group), 1.26–1.29 (m, 14H, –$OC_{12}H_{25}$ group), 1.32 (s, 9H, –$C(CH_3)_3$ group), 1.73 (P, 2H, –CH_2- of –$OC_{12}H_{25}$ group), 4.06 (t, 2H, –OCH_2- of –$OC_{12}H_{25}$), 8.34 (s, 1H, –CH═N group), 7.06–7.83 (4H, first phenyl ring), 7.32–8.16 (4H, second phenyl ring), 7.21–7.64 (4H, third phenyl ring); Elemental analysis of $C_{36}H_{47}NO_3$: Calcu: C; 79.85%, H; 8.68%, O; 8.87%, N; 2.58%, Found: C; 79.78%, H; 8.61%, O; 8.79%, N; 2.52%.

Table 1. Transition temperature of homologous series in °C by POM.

Sr. no	R = n-alkyl group	Transition temperatures in °C				
		Cr	SmC	SmA	N	Iso
1	C_1	·	144.0	160.0	—	182.0
2	C_2	·	142.0	154.0	—	176.0
3	C_3	·	138.0	152.0	—	168.0
4	C_4	·	131.0	147.0	—	162.0
5	C_5	·	114.0	142.0	—	166.0
6	C_6	·	112.0	134.0	—	148.0
7	C_7	·	106.0	128.0	—	138.0
8	C_8	·	102.0	124.0	—	134.0
9	C_{10}	·	95.0	118.0	—	128.0
10	C_{12}	·	93.0	116.0	—	126.0
11	C_{14}	·	98.0	—	112.0	120.0
12	C_{16}	·	94.0	—	104.0	112.0
13	C_{18}	·	86.0	—	96.0	114.0

(Cr = Solid Crystal, SmC = Smectic C phase, SmA = Smectic A phase, N = Nematic phase, Iso = Isotropic phase).

3. Result and discussion

In present studies, we have synthesized total thirteen newly calamatic rod like liquid crystals based on two linking group and *tert* butyl group present in right terminal side while left alkyl chain is varying. In the present investigation, we study the effect of terminal group and varying flexibility on mesomorphism. The liquid crystalline behavior of newly synthesized compounds have been investigated by polarizing optical microscope (POM) and confirm by using differential scanning calorimetry (DSC) analysis.

3.1. POM investigation

It is well known that thermotropic liquid crystalline materials are highly sensitive to their molecular structure. From the chemist's point of view, to design and study the effects of modifications in structure, lateral group, linking group and terminal group on the LCs properties of a synthesized compound. Here, we have synthesized total thirteen homologous in which methane to dodecane chain give SmC, SmA property, while tetradecane to octadecane chain exhibit SmC and nematic property on heating and cooling system. All homologues in present series exhibits mesophase in enantiotropically manner. Transition temperatures of newly synthesized compounds were given in Table 1. The phase diagram of present series plotted against the transition temperature versus number of carbon present in n-alkyl side chain mention in Figure 1. Cr-SmC/I transition curve initially descends at C_{14} homologue and then continued to descending up to C_{18} homologues. Generally, the lengthening of the carbon chain from methyl to octadecyl derivatives revealed an ascending trend in the melting temperatures. This phenomenon can be attributed to the increase in the intermolecular van der waals attraction as the length of the alkoxy side chain increased [34]. SmC/Nm-I transition curve smoothly descends up to C_4 homologue and increases at C_5 homologue and then continued to descending tendency. Odd-even effect is observed at C_5 homologue and disappear for higher homologous which contain longer n-alkyl side chain. SmC–SmA transition curve falling with descending tendency, this is due to the increasing of alkyl spacer in left alkoxy side chain group. SmC–Nm transition curve decreased from C_{14} homologue to C_{18} homologue. Gray et al. explained the increasing in side chain of the molecule and the resulting enhanced anisotropy of the polarizability, increases the intermolecular cohesive forces responsible for higher nematic phase transition curves [34].

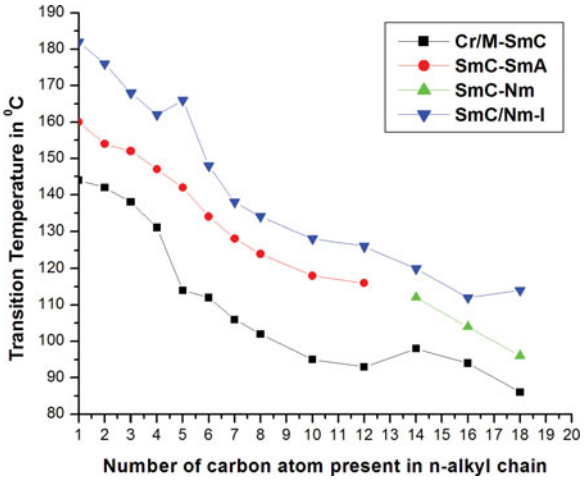

Figure 1. Phase diagram of series.

Texture pattern of nematic phase were determined by miscibility method, which were given in Table 2. In present series, nematic mesophase commences from C_{14} to C_{18} homologous, respectively. The observed texture pattern of present synthesized compounds was compared with standard reported texture patter. Comp. C_{14} shows fan like rod nematic mesophase upon heating and cooling condition, while comp. C_{16} shows some droplets type texture pattern of nematic mesophase and comp. C_{18} exhibit rod like texture pattern of nematic phase.

As a preliminary investigation, the mesophases exhibited by present series was examined by using a polarizing optical microscope. The solid crystalline compounds is sandwiched between the glass slide and coverslip were heated to the isotropic state and heating and cooling rate (2 °C/min), respectively and observing mesophase texture images are shown in Figures 2 and 3. We can clearly see the fan-like texture accompanied by rod texture image of SmA phase of comp. C_{10} at 118 °C given in Figure 2, respectively.

Textures of the compounds of some homologous are shown in Figure 3. Compound C_6 formed the broken fan type SmC phase at 112 °C on heating condition which was further confirmed by DSC analysis. Compound C_3 exhibited a grass like texture pattern of SmC phase at 138 °C upon cooling condition. Compound C_4 displayed texture image of SmC mesophase at 131 °C on heating condition and also reappeared during cooled condition, which was further confirmed by DSC investigation. Compound C_7 formed a needle type texture image of SmC phase at 112 °C enantiotropically manner and it was confirmed by DSC measurement upon heating and cooling cycle. Explicit mesophase assignment was made according to the characteristic textural pattern seen. As can be seen, the lower member (C_1–C_{12}) spacer exhibit SmC and SmA phase, while higher member (C_{14}–C_{18}) exhibit SmC phase and transform into nematic phase on applying further heating. The texture of the mesophase seen through polarizing microscope is signature of SmA mesophase, which has fluid property and broken fan type structures with interlayer spacing. The interlayer attractions are weak and the layers are

Table 2. Nematic phase of compound C_{14}, C_{16}, and C_{18} by miscibility method.

Sr. no.	Homologue	Texture
1	C_{14}	Fan like rod
2	C_{16}	Droplets
3	C_{18}	Threaded

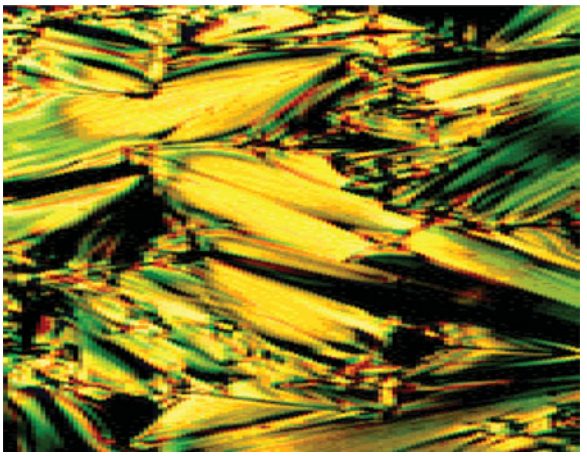

Figure 2. Optical texture micrograph of C_{14} homologue.

moving to slide over one another relatively easily. The flexibility and broadening of molecular length of the layers leads to distortions, which give rise to give the presence of smectic A phase.

The exhibition of nematic phase in higher homologue in present series attributed to the disalignment of molecules of an angle less than ninety degree under the externally exposed thermal vibrations of suitable magnitudes which matches with internal energy stored in a molecule (ΔH) as related to the suitable magnitudes of anisotropic forces of intermolecular

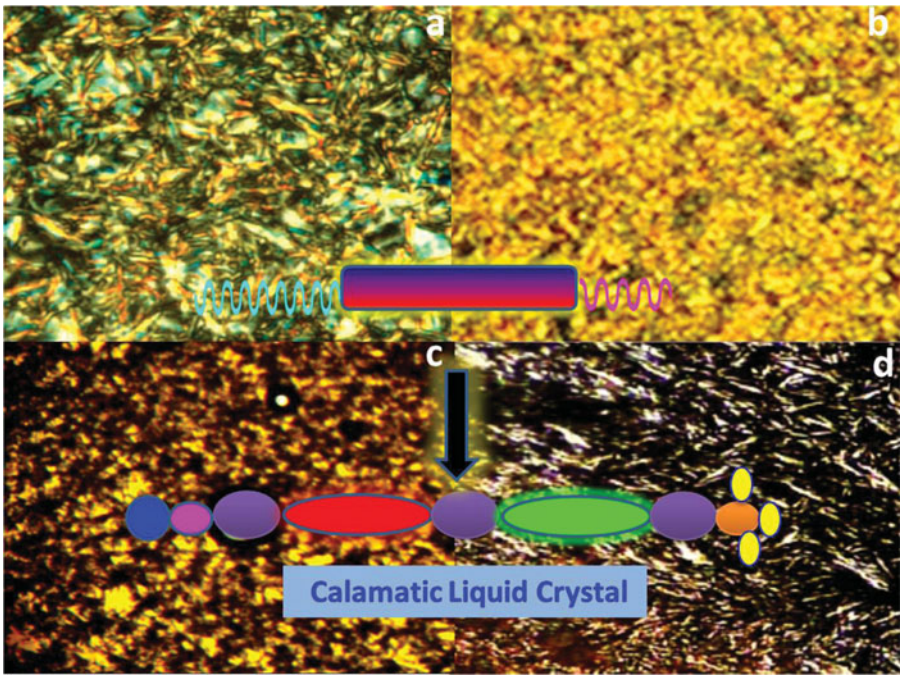

Figure 3. Optical texture micrograph of (a) fan texture of the SmC phase of C_6 homologue; (b) grass texture of the SmC phase C_3 homologue; (c) SmC phase of C_4 homologue; and (d) needle type texture of the C_7 homologue.

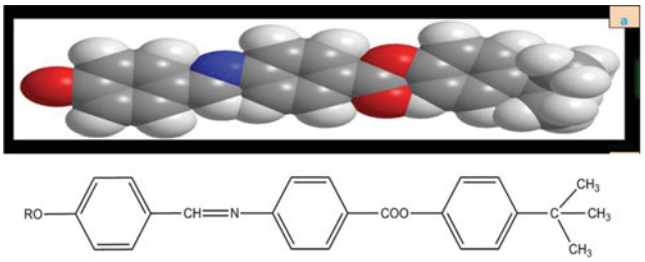

Figure 4. Space filling diagram of present series.

end to end attractions, as a consequence of molecular rigidity and flexibility, which favorably arranges molecules to float on the surface in statistically parallel orientational order to maintain molecular two dimensional array. Thus, nematic mesophase appears on the top of the microscopic observation [35]. First on applying heating, formation of smectic C phase which transform into smectic A in lower alkyl spacer side group and nematic mesophase in higher alkyl spacer group, respectively. It can be seen that, a nematogenic mesophase appeared from and beyond isotropic temperature (N-I), the molecules are randomly oriented in all possible directions with high order of disorder in unexpected manner or with high entropy ($\Delta S = \Delta H/T$). The randomly oriented molecules on cooling from isotropic temperature carefully. Thus, changing in side chain cause variations in intermolecular adhering forces of suitable magnitudes induces and stabilizes nematic mesophase from comp. C_{14} to Comp. C_{18}.

3.2. Thermal stability of mesophase

The space-filling diagram suggests the energy minimize in present series mention in below Figure 4. The geometrical shape of series is rod type, three phenyl ring linked with two linking group azomethine (–CH═N) and ester (–COO) with alkoxy side chain at left terminal part and unaltered *tert* butyl group in all thirteen homologous in present synthesized series. Linking group is one of the factors to exhibiting the smectic phase instead of a nematic phase in synthesized target compounds. The ester linking group favors the lamellar packing due to the dipole–dipole interaction which ultimately generated the smectic phase [34].

Added $-CH_2$ units in side chain increases its molecular length, permanent dipolement, dispersion forces, molecular polarity and polarizability, rigidity and flexibility across the molecular axis with changing the value of enthalpy (ΔH) and keeping rest of the molecular part including $-C(CH_3)_3$ and two linking group azomethine and ester intact throughout the series. Consequently, variation occurs in intermolecular adhesion forces of suitable magnitudes that induce nematic mesophase in higher homologues like C_{14} to C_{18} in homologous series. Broadening of molecular due to presence of nonlinear substituted *tert* butyl group at terminal side exhibiting smectic C as well as nematic mesophase. Presence of oxygen atom in carboxy (–COO) group in the molecules of the series will bump into the nonbonded side of the adjacent hydrogen of the aromatic ring, thereby causing considerable strain on the molecule. This will cause some twist around the carbonyl bond and force the benzene ring out of the plane of the molecule and broadening the molecule [36].

Table 3 shows the average thermal stabilities and mesophase range of newly homologous series (C_1–C_8, C_{10}, C_{12}, C_{14}, C_{16}, and C_{18}). The N–I thermal stability of Series is 115.33 °C. The SmC–SmA thermal stability of Series is 137.5 °C. Thermal stability of SmC–N phase of Series is 92.66 °C. However, the SmA-I thermal stability of Series is 152.8 °C. From the Table 3, it indicates that the average mesophase length of (SmC + N) phase of Series is 22.0 °C and

Table 3. Average thermal and mesophase stabilities of series in °C.

Series	Comp. C_1 to C_{18}
SmC–SmA	137.5
N–I	115.3
SmA–I	152.8
SmC–N	92.66
Total mesophase length (SmC+N)	22.0 to 28.0 C_{14} C_{16}
Commencement of smectic phase	C_1
Commencement of Nematic phase	C_{14}

28.0 °C, respectively. The thermal stability of SmA-I and SmC-SmA phase is higher than the thermal stability of N-I and SmC-N phase in present synthesized Series.

3.2. DSC analysis

DSC is a valuable method for detecting phase transitions. The thermal behavior of novel homologues series were confirmed by using DSC measurement shown in Figure 5. Thermogram is traces in both heating and cooling condition. Microscopic transition temperature values are similar to the DSC data.

On heating condition, C_1 homologue shows two endothermic peaks which is correspondence to the SmC and SmA phase and confirmed by POM study. First endothermic peak observed at 143.22 °C, which indicates the presence of SmC phase. While second endothermic peak observed at 159.98 °C to confirmed the transformation of SmC phase into SmA phase. C_8 homologue shows two significant peaks on heating and cooling condition. First endothermic peak is observed at 105.08 °C and second endothermic peak trace at 131.27 °C on heating

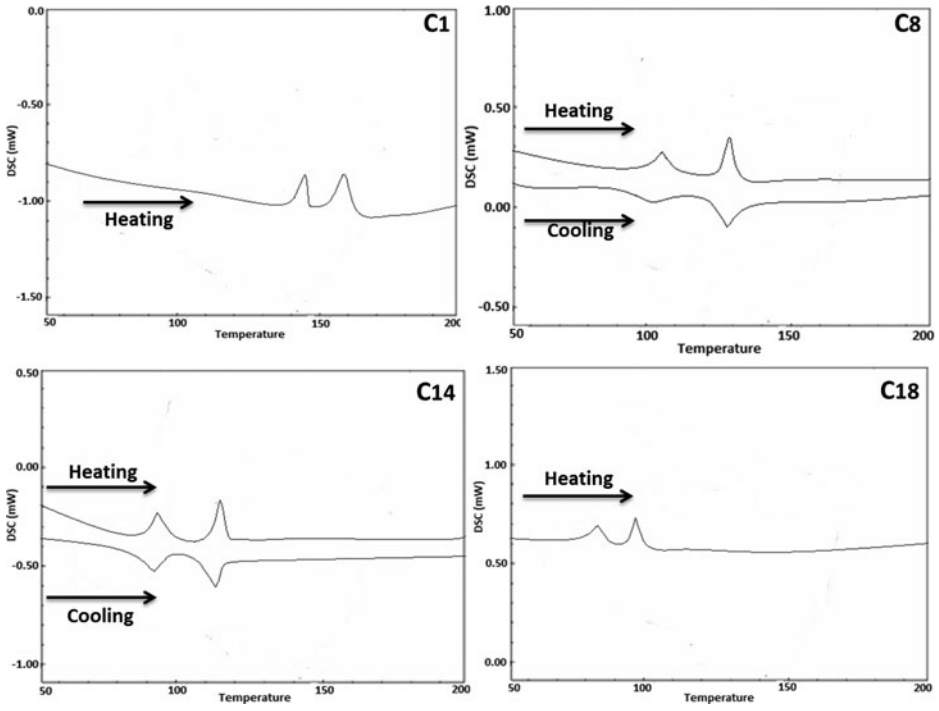

Figure 5. DSC thermogram of (a) C_1, (b) C_8, (c) C_{14}, and (d) C_{18} compound.

Table 4. Transition temperature (°C) and enthalpy (J g^{-1}) and entropy change (J $g^{-1}k^{-1}$) by DSC measurement.

Homologues or comp.	Transition	Heating scan (°C)	Cooling scan (°C)	ΔH (–Jg^{-1})	ΔH (Jg^{-1})	ΔS (J $g^{-1}k^{-1}$)	ΔS (J $g^{-1}k^{-1}$)
C_1	Cr–SmC	143.22	141.12	43.17	34.26	0.1037	0.0827
	SmC–SmA	159.98	156.34	9.24	5.67	0.0213	0.0132
	SmA–I	>170	—	12.10	—	0.0273	—
C_8	Cr–SmC	105.02	101.56	37.92	31.90	0.1003	0.0840
	SmC–SmA	131.12	128.92	9.21	5.45	0.0227	0.0135
	SmA–I	>140	—	11.34	—	0.0274	—
C_{14}	Cr–SmC	96.80	92.12	34.22	22.54	0.0925	0.0617
	SmC–N	114.20	111.83	8.16	4.98	0.0210	0.0129
	N–I	> 120	—	12.43	—	0.0316	—
C_{18}	Cr–SmC	85.91	83.85	32.29	16.43	0.0899	0.0460
	SmC–N	98.23	96.65	7.53	3.54	0.0202	0.0095
	N–I	>110	—	9.62	—	0.0251	—

condition. While on cooling condition, again two endothermic peaks observed at 128.92 °C and 101.56 °C. For C_{14} homologue, two endothermic peaks observed at 96.80 °C and 114.20 °C on heating condition while, on cooling condition, again two endothermic peaks traces at 92.12 °C and 111.83 °C. For C_{18} homologue, it was observed two endothermic peaks trace on heating condition at 85.91 °C and 98.23 °C, respectively. This was further confirmed by POM analysis.

Transition temperature obtained by DSC analysis at heating and cooling condition and the value of enthalpy and entropy is mention in Table 4. Molecules of every homologue randomly oriented in all possible directions with high order of disorder or entropy ($\Delta S = \Delta H/T$) beyond isotropic temperature and the enthalpy value (ΔH). But, at cooled condition, the same from and below isotropic temperature, the mesophase is persisted to appear reversibly at high or lower temperature at observed during heating and cooling condition. The enthalpy values also indicate the crystal to mesophase and mesophase to isotropic transition in compounds C_1, C_8, C_{14}, and C_{18}. The mesophase observed enantiotropically manner in present series.

4. Conclusion

In this article, we have presented the synthesis and characterization as well as the mesomorphic behavior of calamatic rod type homologues series, 4-(tert-butyl) phenyl 4-((4-n-alkoxy benzylidene) amino) benzoate (n = 1 to 8, 10, 12, 14, 16, and 18), which comprised of Schiff base-ester moieties as linking group and alkoxy side chain with terminal tert butyl group. Calamatic rod type compounds with short alkyl spacer exhibits SmC and SmA phases, while in long alkyl spacer exhibits SmC and N mesophases enantiotropically manner. An additional feature found in the present series is that the presence of tert butyl group at terminal side leads more thermal stability of mesophase. In short, the liquid crystalline properties should be driven by the rod-like units and the benzene core act only as a linking unit interconnecting the rods. The Schiff base ester groups are able to increase the linearity and polarizability of the molecule, thus making it possible in the generation of mesomorphism.

Acknowledgments

Authors acknowledge thanks to Dr. R. R. Shah, principal of K. K. Shah Jarodwala Maninagar Science College, Ahmedabad. Author also gratefully thanks to Anuj S Sharma (Chemistry Department, Gujarat

University) and Akshara. P. Shah (Chemistry Department, Mumbai University) for giving fruitful discussions in DSC analysis.

References

[1] (a) Gray, G. W. (1962). *Molecular Structure and the Properties of Liquid Crystals*, Academic Press: London and New York. (b) Hird, M., Toyne, K. J., Gray, G. W., Day, S. E., & Donell, D. G. M. (1993). *Liq.Cryst.*, *15*, 123–150. (c) Hird, M., Goodby, J. W., Gough, N., & Toyne, K. J. (2001). *J. Mater. Chem.*, *11*, 2732–2742. (d) Gray, G. W., Hird, M., Lacey, D., & Toyne, K. J. (1989). *J. Chem. Soc.*, *2*, 2041–2053.
[2] Dave, J. S., Kurian, G., Prajapati, A. P., & Vora, R. A. (1971). *Mol. Cryst. Liq. Cryst.*, *14*, 307.
[3] Isse, A. A., Gennaro, A., & Vianello, E. (1997). *Electrochim. Acta*, *13–14*, 2065–2071.
[4] Liu, X. H., Abser, M., Nurul, B., Duncan, W. (1999). *J. Organomet. Chem.*, *577*, 150–152.
[5] Desai, S. B., Desai, P. B., & Desai, K. R. (2001). *Heterocycl. Commun.*, *7*, 83–90.
[6] Zhao, J. Z., Zhao, B., Xu, W. Q., Liu, J. Z., Wang, Z. M., & Li, Y. X. (2001). *Chem. J. Chin. Univ.*, *22*, 971–975 (in Chinese).
[7] Kelker, H., Scheurle, B. (1969). *Angew. Chem. Int. Ed. Eng. 8*, 884–885.
[8] Matsunaga, Y., Hikosaka, L., Hosono, K., Ikeda, N., Saka-Tani, T., Sekiba, K., Takachi, K., Takahashi, T., & Uemura, Y. (2001). *Mol. Cryst. Liq. Cryst. Sci. Technol. Sect. A*, *369*, 103–116.
[9] Yeap, G. Y., Ha, S. T., Lim, P. L., Boey, P. L., Ito, M. M., Sanehisa, S., & Youhei, Y. (2006). *Liq. Cryst.*, *33*, 205–211.
[10] Campillos, E., Marcos, M., Oriol, L. T., & Serrano, J. L. (1992). *Mole. Cryst. Liq. Cryst. Sci. Technol. Sect. A*, *215*, 127–135.
[11] Dave, J. S., & Prajapati, A. P. (1975). *Pramana*, *Suppl. No.1*, 435.
[12] Dave, J. S., & Kurian, G. (1977). *Mol. Cryst. Liq. Cryst.*, *42*, 193.
[13] Ha, S. T., Foo, K. L., Subramaniam, T., Ito, M. M., Sastry, S. S., & Ong, S. T. (2011). *Ch. Chem. Lett.*, *22*, 1191–1194.
[14] Ooi, Y. H., Yeap, G. Y., & Takeuchi, D. (2013). *J. Mol. Stru.*, *1051*, 361–375.
[15] Ha, S. T., Onga, L. K., Wan Wong, J. P., Yeap, G. Y., Linc, H. C., Onga, S. T., & Koh, T. M. (2009). *Phase Transitions.*, *82*, 387.
[16] Ha, S. T., Ong, L. K., Sivasothy, Y., Yeap, G. Y., Boey, P. L. and Lin, H. C. (2010). *American Journal of Applied Sciences*, *7*(2), 214.
[17] Yeap, G. Y., Ha, S. T., Boey, P. L., & Mahmood, W. A. K. (2006). *Mol. Cryst. Liq. Cryst.*, *452*, 73–90.
[18] Huang, C. C., Hsu, C. C., Chen, L. W., & Cheng, Y. L. (2014). *Soft. Matter.*, *10*, 9343–9351.
[19] Ha, S. T., Ong, L. K., Wong, J. P. W., Yeap, G. Y., Lin, H. C., Ong, S. T., & Koh, T. M. (2009). *Phase Transitions.*, *82*, 387–397.
[20] Yeap, G. W., Ha, S. T., Lim, P. L., Ito, M. M., & Sanehisa, S. (2004). *Mol. Cryst. Liq. Cryst.*, *423*, 73–84.
[21] Dave, J. S., & Kurian, G. (1997). *Mol. Cryst. Liq. Cryst.*, 175–183.
[22] Yelamaggad, C. V., Mathews, M., Nagamani, A., Shankar Rao, D. S., Prasad, S. K., Findeisen, S., & Weissflog, W. (2007). *J. Mater. Chem.*, *17*, 284–298.
[23] Bhola, G. N., & Bhoya, U. C. (2016). *Mol. Cryst. Liq. Cryst.*, *630*, 188–196.
[24] (a) Chaudhari, R. P., Doshi, A. A., & Doshi, A. V. (2013). *Mol. Cryst. Liq. Cryst.*, *582*, 63–71. (b) Chauhan, H. N., & Doshi, A. V. (2013). *Mol. Cryst. Liq. Cryst.*, *570*, 12–19. (c) Chauhan, H. N., Shah, R. R., & Doshi, A. V. (2012). *Mol. Cryst. Liq. Cryst.*, *577*, 36–43. (d) Chaudhari, R. P., & Doshi, A. V. (2012). *Mol. Cryst. Liq. Cryst.*, *569*, 49–56.
[25] Suthar, D. M., & Doshi, A. V. (2012). *Mol. Cryst. Liq. Cryst.*, *569*, 64–71.
[26] Sharma, V. S., & Patel, R. B. (2016). *Mol. Cryst. Liq. Cryst.*, *633*, 37–45.
[27] Sharma, V. S., & Patel, R. B. (2016). *Mol. Cryst. Liq. Cryst.*, *630*, 58–68.
[28] Sharma, V. S., & Patel, R. B. (2016). *Mol. Cryst. Liq. Cryst.*, *630*, 162–171.
[29] (a) Solanki, R. B., Sharma, V. S., & Patel, R. B. (2016). *Mol. Cryst. Liq. Cryst.*, *631*, 107–115. (b) Sharma, V. S., Solanki, R. B., Patel, P. K., & Patel, R. B. (2016). *Mol. Cryst. Liq. Cryst.*, *625*, 137–145. (c) Sharma, V. S., & Patel, R. B. (2015). *ILCPA, Sci. Press*, *58*, 144–153.
[30] (a) Sharma, V. S., & Patel, R. B. (2015), *ILCPA., Sci. Press.*, *59*, 115–123. (b) Sharma, V. S., & Patel, R. B., *ILCPA., Sci. Press.*, (2015), *60*, 182–190. (c) Patel, R. B., Patel, V. R., & Doshi, A. V. (2012). *Mol. Cryst. Liq. Cryst.*, *552*, 3–9. (d) Sharma, V. S., & Patel, R. B. (2016). *WSN.*, *54*, 240–251.

[31] Patel, P. K., & Shah, R. R. (2016). *Mol. Cryst. Liq. Cryst.*, *630*, 130–138.
[32] Furniss, B. S., Hannford, A. J., Smith, P. W. G., & Tatchell, A. R. (Eds.). (1989). *Vogel's Textbook 245 of Practical Organic Chemistry* (4th ed.), *563*, Longmann Singapore Publishers Pvt. Ltd.: Singapore.
[33] Uhood, J. A. (2011). *Int. J. Mol. Sci.*, *12*, 3182–3190.
[34] Gray, G. W. (1962). *Molecular Structure and Properties of Liquid Crystals*, Academic Press: London.
[35] Arora, S. L., Fergason, J. L., & Taylor, T. R. (1970). *J. Org. Chem.*, *35*, 4055–4058.
[36] Sharma, V. S., Patel, R. B., & ILCPA., S. (2016). *69*, 182–191.